Enhanced Domain Decomposition–Model Order Reduction Method for Efficient Broadband Full-Wave Analysis of Multilayer Printed Circuit Boards

Shih-Hao Lee and Jian-Ming Jin

Center for Computational Electromagnetics, Department of Electrical and Computer Engineering
University of Illinois at Urbana-Champaign, Urbana, IL 61801-2991
E-mail: slee213@uiuc.edu, j-jin1@uiuc.edu

I. Abstract

The approximate modal interface–solution space projection is a combined domain decomposition–model order reduction method for an efficient broadband full-wave simulation of multilayer printed circuit boards. The method features a high efficiency and full-wave accuracy for modern electronic designs. In this paper, a number of enhancements to our previously reported algorithm are presented. The enhanced method lifts the restriction on the mesh consistency at subdomain interfaces, and incorporates a coaxial-line model for via-holes as a connection for adjacent interface systems. These enhancements facilitate the mesh generation and improve the modeling flexibility of our numerical method.

II. Introduction

In this paper we present a number of enhancements to our previously reported approximate modal interface–solution space projection (AMI-SSP) method [1], which is a combined domain decomposition–model order reduction (DD-MOR) method for efficient broadband full-wave analysis of multilayer printed circuit boards (PCBs). With the AMI method, a multilayer circuit board can be analyzed layer by layer, leading to a significant improvement in the computational efficiency. The method has been further combined with a multipoint model order reduction method, SSP [2], to enable a fast frequency sweep. The AMI-SSP has been implemented with the finite element method (FEM) for its excellent capability and flexibility in the geometry and material modeling.

The formulation in [1] assumed consistent meshes at the interface (via-holes, for example) between adjacent layers, and therefore, resulted in a restriction on the mesh generation. There is no such a restriction in the enhanced method presented in this paper, and thus the mesh in each layer can be truly generated independently. Furthermore, depending on the geometry and complexity of interconnections, different types of elements or even different orders of basis functions can be applied in different layers. In addition, a multimode coaxial-line model for via-holes is incorporated into the AMI method for connecting two adjacent interface systems. As a result, no mesh needs to be generated for the via-holes on a finite-thickness ground plane.

Some important advantages of the enhanced AMI-SSP can be summarized as follows. 1) The mesh in each layer can be generated independently without the need of consistent meshes on the two sides of an interface. 2) An independent interface system is generated for each layer using the finite element method, and therefore, when the circuit configuration in a certain layer changes, only that layer needs to be re-simulated. 3) The incorporation of a coaxial-line model eliminates the need for thin layers of finite-element mesh in a via-hole region. The thickness of a ground plane is equivalent to the length of a coaxial line and can be arbitrarily changed without regenerating the interface systems for related layers.

III. Approximate Modal Interface Method

Consider a multilayer structure shown in Fig. 1. The solid and dashed lines represent planar metallization and apertures (S_1 – S_5, including via-holes and ports), respectively. On each aperture an unknown magnetic field $\vec{H}_S$ is assumed, and thus the FEM matrix equation for Layer 1 can be expressed as

$$\begin{bmatrix} \boldsymbol{K}_{S_1S_1} & \boldsymbol{0} & \boldsymbol{K}_{S_1V_1} \\ \boldsymbol{0} & \boldsymbol{K}_{S_2S_2} & \boldsymbol{K}_{S_2V_1} \\ \boldsymbol{K}_{V_1S_1} & \boldsymbol{K}_{V_1S_2} & \boldsymbol{K}_{V_1V_1} \end{bmatrix} \begin{pmatrix} \boldsymbol{E}_{S_1} \\ \boldsymbol{E}_{S_2} \\ \boldsymbol{E}_{V_1} \end{pmatrix} = \boldsymbol{K}^{(1)} \begin{pmatrix} \boldsymbol{E}_{S_1} \\ \boldsymbol{E}_{S_2} \\ \boldsymbol{E}_{V_1} \end{pmatrix} = \begin{pmatrix} \boldsymbol{b}_{S_1} \\ \boldsymbol{b}_{S_2} \\ \boldsymbol{0} \end{pmatrix} \tag{1}$$

where $\boldsymbol{K}^{(1)}$ denotes the FEM matrix of Layer 1. Excitation vectors $\boldsymbol{b}_{S_1}$ and $\boldsymbol{b}_{S_2}$ result from the discretization of

$$B_i(\vec{E}) = \iint_{S_i} jk_0 Z_0 \vec{E}\cdot(\hat{n}\times\vec{H}_{S_i})dS = \sum_{k=1}^{m_i} c_{ik} \iint_{S_i} \frac{1}{\mu_r}\vec{E}\cdot(\gamma_k \vec{e}_{ti,k} + \nabla_t e_{zi,k})dS \equiv \sum_{k=1}^{m_i} c_{ik} B_{ik}(\vec{E}) \quad i=1,2 \tag{2}$$

where $\vec{H}_S$ has been expanded with modal fields of the associated apertures. c_{ik} is a modal combination coefficient associated with the kth mode of S_i, and m_i is the number of modes used in the modal expansion. Thus,

$$\boldsymbol{b}_{S_i} = \boldsymbol{A}_i \boldsymbol{c}_i \quad i=1,2 \tag{3}$$

where the kth column of $\boldsymbol{A}_i$ results from the discretization of $B_{ik}(\vec{E})$, and $\boldsymbol{c}_i$ is an array of combination coefficients which will be determined. Substituting (3) into (1), the field solution can be determined to be

$$\begin{pmatrix} \boldsymbol{E}_{S_1} \\ \boldsymbol{E}_{S_2} \\ \boldsymbol{E}_{V_1} \end{pmatrix} = \boldsymbol{K}^{(1)^{-1}} \begin{bmatrix} \boldsymbol{A}_1 & \boldsymbol{0} \\ \boldsymbol{0} & \boldsymbol{A}_2 \\ \boldsymbol{0} & \boldsymbol{0} \end{bmatrix} \begin{pmatrix} \boldsymbol{c}_1 \\ \boldsymbol{c}_2 \end{pmatrix} = \boldsymbol{K}^{(1)^{-1}} \begin{bmatrix} \boldsymbol{a}_1 & \boldsymbol{a}_2 \end{bmatrix} \begin{pmatrix} \boldsymbol{c}_1 \\ \boldsymbol{c}_2 \end{pmatrix} = \begin{bmatrix} \boldsymbol{x}_1 & \boldsymbol{x}_2 \end{bmatrix} \begin{pmatrix} \boldsymbol{c}_1 \\ \boldsymbol{c}_2 \end{pmatrix} \tag{4}$$

from which we obtain the following interface system for Layer 1

$$\begin{pmatrix} \boldsymbol{E}_{S_1} \\ \boldsymbol{E}_{S_2} \end{pmatrix} = \begin{bmatrix} \boldsymbol{m}_{11}^{(1)} & \boldsymbol{m}_{12}^{(1)} \\ \boldsymbol{m}_{21}^{(1)} & \boldsymbol{m}_{22}^{(1)} \end{bmatrix} \begin{pmatrix} \boldsymbol{c}_1 \\ \boldsymbol{c}_2 \end{pmatrix}. \tag{5}$$

Once $\boldsymbol{x}_1$ and $\boldsymbol{x}_2$ are obtained, the system matrix $\boldsymbol{K}^{(1)}$ and its factorization matrices will not be used again and can all be deleted from the memory. The interface system for Layer 2 can similarly be derived as

$$\begin{pmatrix} \boldsymbol{E}_{S_2} \\ \boldsymbol{E}_{S_3} \\ \boldsymbol{E}_{S_4} \end{pmatrix} = \begin{bmatrix} \boldsymbol{m}_{11}^{(2)} & \boldsymbol{m}_{12}^{(2)} & \boldsymbol{m}_{13}^{(2)} \\ \boldsymbol{m}_{21}^{(2)} & \boldsymbol{m}_{22}^{(2)} & \boldsymbol{m}_{23}^{(2)} \\ \boldsymbol{m}_{31}^{(2)} & \boldsymbol{m}_{32}^{(2)} & \boldsymbol{m}_{33}^{(2)} \end{bmatrix} \begin{pmatrix} \boldsymbol{c}_2 \\ \boldsymbol{c}_3 \\ \boldsymbol{c}_4 \end{pmatrix}. \tag{6}$$

Five equations are required for unique determination of $\boldsymbol{c}_i, i = 1,2,\ldots,5$. Two of the equations come from the fact that two adjacent interface systems should yield the same interface fields. If we have, however, inconsistent meshes at the interface, then the projections to the modal fields are required to be the same. For example, at S_2,

$$\boldsymbol{A}_2^{uH}(\boldsymbol{m}_{21}^{(1)}\boldsymbol{c}_1 + \boldsymbol{m}_{22}^{(1)}\boldsymbol{c}_2) = \boldsymbol{A}_2^{\ell H}(\boldsymbol{m}_{11}^{(2)}\boldsymbol{c}_2 + \boldsymbol{m}_{12}^{(2)}\boldsymbol{c}_3 + \boldsymbol{m}_{13}^{(2)}\boldsymbol{c}_4) \tag{7}$$

is enforced, where $\boldsymbol{A}_2^u$ and $\boldsymbol{A}_2^\ell$ are modal fields obtained with possibly different meshes on the upper and lower sides of S_2, respectively, and their phases have been calibrated. The projections in (7) results in vectors with lengths equal to the number of modes. Hence the only requirement is that the same number of modes has to be used on both sides of an interface.

The other three equations can be derived from the interface systems together with the use of the port boundary conditions at the three ports, as has been described in [1]. Finally, we obtain a global interface system

$$\begin{bmatrix} \boldsymbol{A}_1^H\boldsymbol{P}_1\boldsymbol{m}_{11}^{(1)} - \boldsymbol{A}_1^H\boldsymbol{A}_1 & \boldsymbol{A}_1^H\boldsymbol{P}_1\boldsymbol{m}_{12}^{(1)} & & & \\ \boldsymbol{A}_2^{uH}\boldsymbol{m}_{21}^{(1)} & \boldsymbol{A}_2^{uH}\boldsymbol{m}_{22}^{(1)} - \boldsymbol{A}_2^{\ell H}\boldsymbol{m}_{11}^{(2)} & -\boldsymbol{A}_2^{\ell H}\boldsymbol{m}_{12}^{(2)} & -\boldsymbol{A}_2^{\ell H}\boldsymbol{m}_{13}^{(2)} & \\ & \boldsymbol{A}_3^H\boldsymbol{P}_3\boldsymbol{m}_{21}^{(2)} & \boldsymbol{A}_3^H\boldsymbol{P}_3\boldsymbol{m}_{22}^{(2)} - \boldsymbol{A}_3^H\boldsymbol{A}_3 & \boldsymbol{A}_3^H\boldsymbol{P}_3\boldsymbol{m}_{23}^{(2)} & \\ & \boldsymbol{A}_4^{uH}\boldsymbol{m}_{31}^{(2)} & \boldsymbol{A}_4^{uH}\boldsymbol{m}_{32}^{(2)} & \boldsymbol{A}_4^{uH}\boldsymbol{m}_{33}^{(2)} - \boldsymbol{A}_4^{\ell H}\boldsymbol{m}_{11}^{(3)} & -\boldsymbol{A}_4^{\ell H}\boldsymbol{m}_{12}^{(3)} \\ & & & \boldsymbol{A}_5^H\boldsymbol{P}_5\boldsymbol{m}_{21}^{(3)} & \boldsymbol{A}_5^H\boldsymbol{P}_5\boldsymbol{m}_{22}^{(3)} - \boldsymbol{A}_5^H\boldsymbol{A}_5 \end{bmatrix} \begin{pmatrix} \boldsymbol{c}_1 \\ \boldsymbol{c}_2 \\ \boldsymbol{c}_3 \\ \boldsymbol{c}_4 \\ \boldsymbol{c}_5 \end{pmatrix} = \begin{pmatrix} \boldsymbol{b}_1 \\ \\ \boldsymbol{b}_3 \\ \\ \boldsymbol{b}_5 \end{pmatrix} \tag{8}$$

where $\boldsymbol{P}_i$ and $\boldsymbol{b}_i$ are the port-boundary-condition matrix and the dominant-mode excitation vector of each port, respectively, and the dimension of the system is equal to the total number of modes used in the modal expansion. Solving this global interface system yields the arrays of combination coefficients, with which we can calculate all the aperture fields from the interface systems and then extract S-parameters.

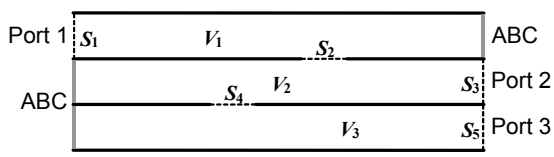

Fig. 1. Side view of a multilayer structure.

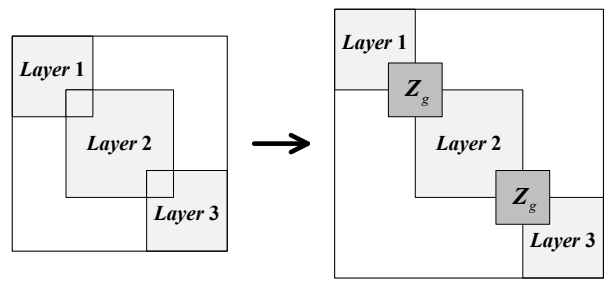

Fig. 2. Global interface systems before and after incorporating the coaxial line models for via-holes.

IV. Incorporation of Coaxial-Line Models

A projected interface system can be viewed as a generalized impedance matrix since it relates the coefficients of modal magnetic fields to the projections of electric field at each aperture. If the approach described in Section III is applied to a (two-port) coaxial line, then the projected interface system can be written as

$$\begin{bmatrix} \boldsymbol{A}_1^H \boldsymbol{E}_1 \\ \boldsymbol{A}_2^H \boldsymbol{E}_1 \end{bmatrix} = \begin{bmatrix} \boldsymbol{A}_1^H \boldsymbol{e}_{t1} & \boldsymbol{0} \\ \boldsymbol{0} & \boldsymbol{A}_2^H \boldsymbol{e}_{t2} \end{bmatrix} \begin{bmatrix} \boldsymbol{V}_1 \\ \boldsymbol{V}_2 \end{bmatrix} = \begin{bmatrix} \boldsymbol{A}_1^H \boldsymbol{m}_{11} & \boldsymbol{A}_1^H \boldsymbol{m}_{12} \\ \boldsymbol{A}_2^H \boldsymbol{m}_{21} & \boldsymbol{A}_2^H \boldsymbol{m}_{22} \end{bmatrix} \begin{bmatrix} \boldsymbol{I}_1 \\ \boldsymbol{I}_2 \end{bmatrix} \equiv \boldsymbol{Z}_g \begin{bmatrix} \boldsymbol{I}_1 \\ \boldsymbol{I}_2 \end{bmatrix} \tag{9}$$

where $\boldsymbol{e}_{t1}$ and $\boldsymbol{e}_{t2}$ are the transverse components of modal electric fields at ports 1 and 2, respectively, $\boldsymbol{V}$ and $\boldsymbol{I}$ are used to denote the modal coefficients, and $\boldsymbol{Z}_g$ is a generalized impedance matrix. As a result,

$$\begin{bmatrix} \boldsymbol{V}_1 \\ \boldsymbol{V}_2 \end{bmatrix} = \begin{bmatrix} \boldsymbol{A}_1^H \boldsymbol{e}_{t1} & \boldsymbol{0} \\ \boldsymbol{0} & \boldsymbol{A}_2^H \boldsymbol{e}_{t2} \end{bmatrix}^{-1} \boldsymbol{Z}_g \begin{bmatrix} \boldsymbol{I}_1 \\ \boldsymbol{I}_2 \end{bmatrix} \equiv \boldsymbol{Z} \begin{bmatrix} \boldsymbol{I}_1 \\ \boldsymbol{I}_2 \end{bmatrix} \tag{10}$$

where $\boldsymbol{Z}$ is an impedance matrix. Our objective is to obtain $\boldsymbol{Z}_g$ without meshing the volume of the coaxial-line. This can be achieved by first forming a multimode coaxial line model in the form of a scattering matrix $\boldsymbol{S}$ using the modal propagation constants (numerically obtained with $\boldsymbol{e}_t$) and the length of the line. From $\boldsymbol{S}$ we can calculate our desired generalized impedance matrix as

$$\boldsymbol{Z}_g = \begin{bmatrix} \boldsymbol{A}_1^H \boldsymbol{e}_{t1} & \boldsymbol{0} \\ \boldsymbol{0} & \boldsymbol{A}_2^H \boldsymbol{e}_{t2} \end{bmatrix} \boldsymbol{Z} = \begin{bmatrix} \boldsymbol{A}_1^H \boldsymbol{e}_{t1} & \boldsymbol{0} \\ \boldsymbol{0} & \boldsymbol{A}_2^H \boldsymbol{e}_{t2} \end{bmatrix} (\boldsymbol{I} + \boldsymbol{S})(\boldsymbol{I} - \boldsymbol{S})^{-1} . \tag{11}$$

Then $\boldsymbol{Z}_g$ is added on to the global interface system as illustrated in Fig. 2. Note that originally the interface between two adjacent layers is located at the middle of the thickness in each via-hole. Now this interface is split into the two port surfaces of a coaxial line. The submatrices no longer overlap but are coupled by $\boldsymbol{Z}_g$.

V. Numerical Example

Fig. 3 shows two pairs of differential vias connected by coupled striplines in the first layer of a lossy three-layer PCB [3]. An air layer bounded by the absorbing boundary condition is attached to the bottom of the structure for simulating the open space. By exploiting the geometrical symmetry, the discretization of the reduced problem with edge elements yields 187,651 unknowns. The entire AMI-SSP process took about 10 minutes to yield *S*-parameters at 400 frequencies (0.1 – 20 GHz), and the peak memory usage is 1.7 GB. All the computations were carried out on a desktop with a 2.66-GHz Intel Pentium IV processor.

Fig. 4 displays the simulated S_{21} (solid line) with inconsistent meshes at the interfaces as compared to the measured result (dotted line) [3]. Good agreement is observed. Also shown in Fig. 4 is the result obtained by using different orders of basis functions in different layers (dashed line). Specifically speaking, we still use the first-order vector basis in the first layer for there exists a much denser mesh for modeling the minute parts of the inter-connection. On the other hand, second-order vector basis is employed in the other layers (with a reduced mesh

density). Better accuracy of this mixed-order simulation can be observed.

The original thickness of the ground planes is 0.03 mm. Now we use the coaxial-line model described in Section IV to replace the finite-element mesh in the via-holes. It can be seen in Fig. 5 that the dashed line (using the coaxial-line model) totally coincides with the solid line (original solution). We further increase the thickness of the ground planes to 0.12 mm, and the dashed and solid lines still coincide with each other. This verifies the effectiveness of the coaxial-line model in the AMI method.

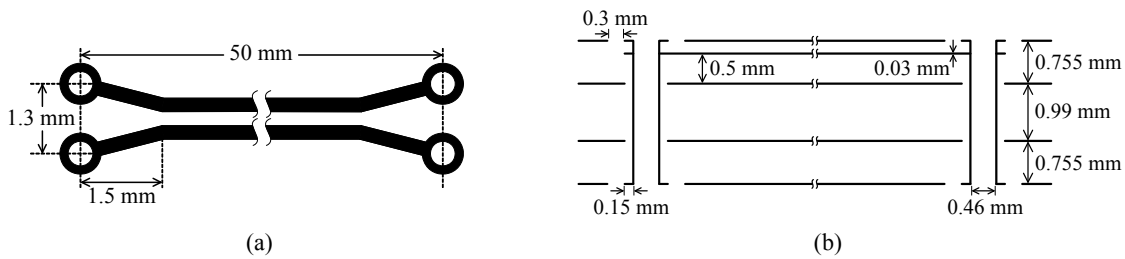

Fig. 3. (a) Top view of the differential via structure [3]. (b) Side view.

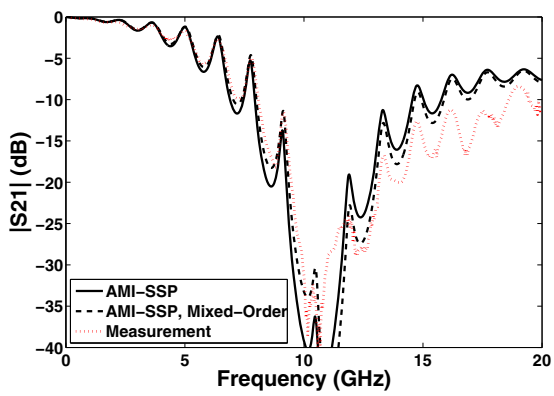

Fig. 4. Comparison of S_{21} obtained from AMI-SSP with different orders of elements and from the measurement [3].

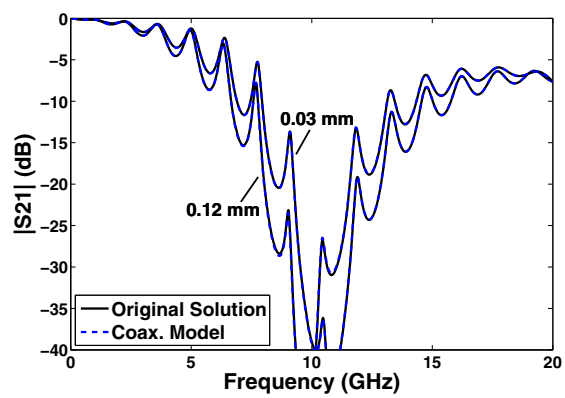

Fig. 5. S_{21} of the differential via structure obtained with and without applying the coaxial-line model.

VI. Conclusion

We have demonstrated and validated the proposed enhancements to the AMI method. The restriction on the interface mesh consistency has been completely eliminated and even different orders of elements can be used in different layers. The finite-element meshes in via-holes can be replaced by coaxial-line models, which proved to be highly accurate regardless of the thickness of a ground plane. The number of unknowns is of course reduced and the time for matrix factorization is also reduced. Yet the most important advantages of these enhancements comprise the facilitation of model creation and mesh generation, as well as the improved flexibility of the AMI method.

References

[1] S. H. Lee and J. M. Jin, "Efficient full-wave analysis of multilayer interconnection structures using a novel domain decomposition–model order reduction method," in *IEEE 16th Conference on Electrical Performance of Electronic Packaging*, Atlanta, Oct. 2007.

[2] S. H. Lee and J. M. Jin, "Adaptive solution space projection for fast and robust wideband finite-element simulation of microwave components," *IEEE Microwave and Wireless Component Letters*, vol. 17, pp. 474-476, July 2007.

[3] E. Laermans, J. De Geest, D. De Zutter, F. Olyslager, S. Sercu, and D. Morlion, "Modeling complex via hole structures," *IEEE Trans. Adv. Packag.*, vol. 25, pp. 206–214, May 2002.